11th World Congress on Computational Mechanics (WCCM XI)
5th European Conference on Computational Mechanics (ECCM V)
6th European Conference on Computational Fluid Dynamics (ECFD VI)
E. Oñate, J. Oliver and A. Huerta (Eds)

DESCENT OF A SOLID DISK IN QUIESCENT FLUID SIMULATED USING INCOMPRESSIBLE SMOOTHED PARTICLE HYDRODYNAMICS

NIMA TOFIGHI[*†], MURAT OZBULUT[†], AMIN RAHMAT[†], MEHMET YILDIZ[†] AND JAMES J. FENG[‡]

[†]Faculty of Engineering and Natural Sciences (FENS), Sabanci University,
Orhanli, Tuzla, 34956 Istanbul, Turkey
e-mails: nima@sabanciuniv.edu
ozbulut@sabanciuniv.edu
arahmat@sabanciuniv.edu
meyildiz@sabanciuniv.edu

[‡]Department of Mathematics, University of British Columbia,
Vancouver, BC V6T 1Z2, Canada
e-mail: jfeng@math.ubc.ca

Key words: Smoothed Particle Hydrodynamics, Fluid Solid Interaction, Single Domain Approach, Disk Descent

Abstract. Incompressible smoothed particle hydrodynamics method has been used to simulate the descent of a solid disk in quiescent medium under gravitational acceleration. Using a single domain approach, we have studied the effects of viscosity ratio and interpolation scheme. Comparison with available data in the literature shows quantitative agreement.

1 INTRODUCTION

The interaction of a solid body with a fluid environment is one of the most common flow features in nature and industry covering a gamut of phenomena from the motion of a school of fish within water to rotating blades of a pump. As such, it has been the subject of interest for many studies involving computational fluid dynamics [1–3]. Particle methods are particularly suitable for these problems as discretization points may move with the solid body and conform to the boundaries [4–6].

In this study, a two–dimensional Incompressible Smoothed Particle Hydrodynamics (ISPH) scheme based on the projection method proposed by Cummins and Rudmann [7] is developed to simulate the interaction between a passive solid object and the surrounding fluid. The scheme is based on a single domain model where all phases within the system

are treated as fluids with different viscosities [1, 8] while the solid phase is represented by particles of fixed relative configuration. As such, the value of viscosity chosen and the scheme of interpolation used to transition between the solid and fluid phases are of utmost importance in accurate representation of the physical phenomenon. Weighted harmonic averaging and a viscosity ratio of 100 are observed to provide satisfactory results during the simulations and are employed to perform a simulation of a solid disk settling in a quiescent fluid under gravity. The results of the simulations are in agreement with literature data.

2 GOVERNING EQUATIONS

Equations governing an incompressible flow may be written in non–dimensional form as

$$\boldsymbol{\nabla} \cdot \mathbf{u} = 0, \tag{1}$$

$$\frac{\mathrm{D}\mathbf{u}}{\mathrm{D}t} = -\boldsymbol{\nabla} p + \frac{1}{\mathrm{Re}} \boldsymbol{\nabla} \cdot \boldsymbol{\tau}, \tag{2}$$

where $\mathbf{u}$ is the velocity vector, p is pressure, ρ is density, t is time and $\mathrm{D}/\mathrm{D}t = \partial/\partial t + \mathbf{u} \cdot \boldsymbol{\nabla}$ represents the material time derivative. Here, $\boldsymbol{\tau}$ and Re are viscous stress tensor and Reynolds number, respectively. Viscous stress tensor is defined as

$$\boldsymbol{\tau} = \mu \left[\boldsymbol{\nabla} \mathbf{u} + (\boldsymbol{\nabla} \mathbf{u})^{\dagger} \right], \tag{3}$$

where μ denotes viscosity and superscript $\square^{\dagger}$ represents the transpose operation. Non–dimensional values are formed using the following scales

$$\begin{aligned} &\mathbf{x} = \mathbf{x}^*/d, \quad \rho = \rho^*/\rho_f, \quad \mathbf{u} = \mathbf{u}^*/\sqrt{gd}, \quad t = t^*\sqrt{g/d}, \\ &p = \left(p^* - \rho g y\right) / \left(\rho g d\right), \quad \mathcal{R} = \rho_s/\rho_f, \quad \mathcal{M} = \mu_s/\mu_f, \end{aligned} \tag{4}$$

leading to a Reynolds number defined as

$$\mathrm{Re} = \frac{\rho_f \sqrt{g d^3}}{\mu_f}, \tag{5}$$

where g is the gravitational acceleration in vertical direction y and d denotes disk diameter. An asterisk marks dimensional variables whereas subscripts $\square_s$ and $\square_f$ denote fluid and solid phases, respectively.

To distinguish between different phases, a color function $\hat{c}$ is defined such that it assumes a value of zero for one phase and unity for the other. The color function is then smoothed out across the phase boundaries as

$$c_{\mathrm{i}} = \sum_{\mathrm{j}=1}^{J_n} \frac{\hat{c}_{\mathrm{j}} W_{\mathrm{ij}}}{\psi_{\mathrm{i}}} \tag{6}$$

to ensure smooth transition between the properties of each phase when used for their interpolation. Here, $\psi_{\mathrm{i}} = \sum_{\mathrm{j}=1}^{J_n} W_{\mathrm{ij}}$, is the number density of SPH particle i, calculated as the sum of interpolation kernel of neighboring particles i and j over all neighbors of particle i, J_n. Interpolation kernel, $W(r_{\mathrm{ij}}, h)$, is a function of the magnitude of distance vector, $\mathbf{r}_{\mathrm{ij}} = \mathbf{r}_{\mathrm{i}} - \mathbf{r}_{\mathrm{j}}$, between particle of interest i and its neighboring particles j and h, the smoothing length [9, 10]. Interpolation of phase properties may be carried out as Weighted Arithmetic Mean (WAM),

$$\phi_{\mathrm{i}} = \phi_s c_{\mathrm{i}} + \phi_f \left(1 - c_{\mathrm{i}}\right), \tag{7}$$

or Weighted Harmonic Mean (WHM),

$$\frac{1}{\phi_{\mathrm{i}}} = \frac{c_{\mathrm{i}}}{\phi_s} + \frac{1 - c_{\mathrm{i}}}{\phi_f}, \tag{8}$$

where ϕ may denote viscosity or density.

All phases are treated as liquids and are evolved through equations 1 and 2. However, to impose rigidity constraints, we use the current velocity of the solid particles to compute a center–of–mass velocity and an angular velocity for the solid object:

$$\mathbf{u}_s^t = \frac{1}{J_s} \sum_{\mathrm{j}=1}^{J_s} \mathbf{u}_{\mathrm{j}}, \tag{9}$$

$$\mathbf{u}_s^r = \frac{1}{I_s} \sum_{\mathrm{j}=1}^{J_s} \mathbf{u}_{\mathrm{j}} \times \mathbf{r}_{\mathrm{j}s}, \tag{10}$$

and then assign an individual velocity to each solid particle according to rigid body motion:

$$\mathbf{u}_{\mathrm{i}} = \mathbf{u}_s^t + \mathbf{u}_s^r \times \mathbf{r}_{\mathrm{i}s}. \tag{11}$$

Here, $\mathbf{r}_{\mathrm{i}s} = \mathbf{r}_{\mathrm{i}} - \mathbf{r}_s$ where $\mathbf{r}_s$ denotes the solid object's center of mass, J_s is the number of particles present in the solid phase and I_s is the solid object's moment of inertia about its center of mass.

A predictor-correcter scheme is employed to advance the governing equations of flow in time using a first-order Euler approach with variable timestep according to Courant-Friedrichs-Lewy condition, $\Delta t = C_{CFL} h / u_{max}$, where u_{max} is the largest particle velocity magnitude and C_{CFL} is taken to be equal to 0.25. In the predictor step all the variables are advanced to their intermediate form using the following relations,

$$\mathbf{r}_{\mathrm{i}}^* = \mathbf{r}_{\mathrm{i}}^{(n)} + \mathbf{u}_{\mathrm{i}}^{(n)} \Delta t + \boldsymbol{\delta} \mathbf{r}_{\mathrm{i}}^{(n)}, \tag{12}$$

$$\mathbf{u}_{\mathrm{i}}^* = \mathbf{u}_{\mathrm{i}}^{(n)} + \boldsymbol{\nabla} \cdot \boldsymbol{\tau}_{\mathrm{i}}^{(n)} \Delta t, \tag{13}$$

$$\psi_{\mathrm{i}}^* = \psi_{\mathrm{i}}^{(n)} - \Delta t \psi_{\mathrm{i}}^{(n)} \left(\boldsymbol{\nabla} \cdot \mathbf{u}_{\mathrm{i}}^*\right), \tag{14}$$

where starred variables represent intermediate values and superscript (n) denotes values at the n^{th} time step. The artificial particle displacement vector in (12), $\boldsymbol{\delta}\mathbf{r}_{\mathrm{i}}$, is defined as in [11] and a constant value of 0.06 is used.

Using intermediate values, pressure at the next time step is found by solving the Poisson equation which is then followed by corrections in position and velocity of the particles, completing the temporal transition:

$$\boldsymbol{\nabla}\cdot\left(\frac{1}{\rho_{\mathrm{i}}^{*}}\boldsymbol{\nabla}p_{\mathrm{i}}^{(n+1)}\right)=\frac{\boldsymbol{\nabla}\cdot\mathbf{u}_{\mathrm{i}}^{*}}{\Delta t}, \tag{15}$$

$$\mathbf{u}_{\mathrm{i}}^{(n+1)}=\mathbf{u}_{\mathrm{i}}^{*}-\frac{1}{\rho_{\mathrm{i}}}\boldsymbol{\nabla}p_{\mathrm{i}}^{(n+1)}\Delta t, \tag{16}$$

$$\mathbf{r}_{\mathrm{i}}^{(n+1)}=\mathbf{r}_{\mathrm{i}}^{(n)}+\frac{1}{2}\left(\mathbf{u}_{\mathrm{i}}^{(n)}+\mathbf{u}_{\mathrm{i}}^{(n+1)}\right)\Delta t+\boldsymbol{\delta}\mathbf{r}_{\mathrm{i}}^{(n)}. \tag{17}$$

In these equations, the rigidity constraints (9–11) are implemented after each velocity update.

Boundary conditions are enforced through MBT method described in [12] while first derivative and Laplace operator are approximated through the following expressions

$$\frac{\partial f_{\mathrm{i}}^{m}}{\partial x_{\mathrm{i}}^{k}}a_{\mathrm{i}}^{kl}=\sum_{\mathrm{j}}\frac{1}{\psi_{\mathrm{j}}}\left(f_{\mathrm{j}}^{m}-f_{\mathrm{i}}^{m}\right)\frac{\partial W_{\mathrm{ij}}}{\partial x_{\mathrm{i}}^{l}}, \tag{18}$$

$$\frac{\partial^{2} f_{\mathrm{i}}^{m}}{\partial x_{\mathrm{i}}^{k}\partial x_{\mathrm{i}}^{k}}a_{\mathrm{i}}^{ml}=8\sum_{\mathrm{j}}\frac{1}{\psi_{\mathrm{j}}}\left(f_{\mathrm{i}}^{m}-f_{\mathrm{j}}^{m}\right)\frac{r_{\mathrm{ij}}^{m}}{r_{\mathrm{ij}}^{2}}\frac{\partial W_{\mathrm{ij}}}{\partial x_{\mathrm{i}}^{l}}. \tag{19}$$

Here, $a_{\mathrm{i}}^{kl}=\sum_{\mathrm{j}}\frac{r_{\mathrm{ij}}^{k}}{\psi_{\mathrm{j}}}\frac{\partial W_{\mathrm{ij}}}{\partial x_{\mathrm{i}}^{l}}$ is a corrective second rank tensor that eliminates particle inconsistencies [11]. Left hand side of (15) is discretized as

$$\frac{\partial^{2} f_{\mathrm{i}}^{m}}{\partial x_{\mathrm{i}}^{k}\partial x_{\mathrm{i}}^{k}}\left(2+a_{\mathrm{i}}^{kk}\right)=8\sum_{\mathrm{j}}\frac{1}{\psi_{\mathrm{j}}}\left(f_{\mathrm{i}}^{m}-f_{\mathrm{j}}^{m}\right)\frac{r_{\mathrm{ij}}^{k}}{r_{\mathrm{ij}}^{2}}\frac{\partial W_{\mathrm{ij}}}{\partial x_{\mathrm{i}}^{k}}. \tag{20}$$

3 GEOMETRY AND PARAMETERS

A solid disk is allowed to descend from rest under gravity in quiescent medium. Our computational domain consists of an 8×24 rectangle discretized by 62854 particles positioned along concentric circles at uniform radial spacing around the solid disk's center. The radial spacing is chosen such that 10 circles fit inside the disk while the number of particles along each of these circles vary to keep the overall inter–particle spacing across the computational domain as uniform as possible. The disk is positioned at $(4, 16)$ having a unit diameter (figure 1).

The proposed scheme for simulation of passive solids treats all phases as liquids of different viscosities initially, only to differentiate the solid phase by the rigid–body constraints (9–11) afterwards. As such, the viscosity ratio between the phases and the way

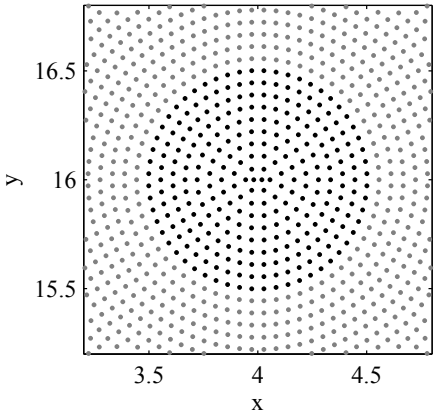

Figure 1: Closeup view of initial particle distribution at the vicinity of the solid disk. Black points denote solid particles whereas gray points are fluid particles.

Table 1: Viscosity ratio and interpolation scheme for all test cases

Case	C1	C3	C10	C30	C100	C300	C1000	C100A
$\mathcal{M}$	1	3	10	30	100	300	1000	100
Interp. Sch.	WHM	WHM	WHM	WHM	WHM	WHM	WHM	WAM

the transitions and interpolations are carried out have significant effects on the results obtained. A series of simulations have been carried out to asses the aforementioned effects. Table 1 provides viscosity ratio and interpolation scheme of the test cases simulated. Reynolds number is set to 39.1 and a density ratio of 1.25 is chosen for the simulations.

4 RESULTS

In this section, the results for simulation of the descent of the solid disk at different viscosity ratios and averaging schemes are presented.

As the proposed scheme treats all phases as liquids and applies rigidity constraints afterwards, the velocities obtained by individual solid particles during liquid phase treatment affects the overall motion of the solid after the constraints are applied. It is expected to achieve a solid-like behavior at large enough viscosities. However, a threshold has to be set as larger viscosity ratios may destabilize the simulation. To this end, viscosity ratios of 1 through 1000 are tested (table 1). Figure 2 presents vertical position and vertical velocity of the solid disk's center of mass versus time. The general trend consists of an acceleration stage, descent at constant velocity and deceleration when approaching the bottom of the domain. It appears that the profiles converge at around a viscosity ratio of 100. To demonstrate the difference between disk positions better, figure 3 provides con-

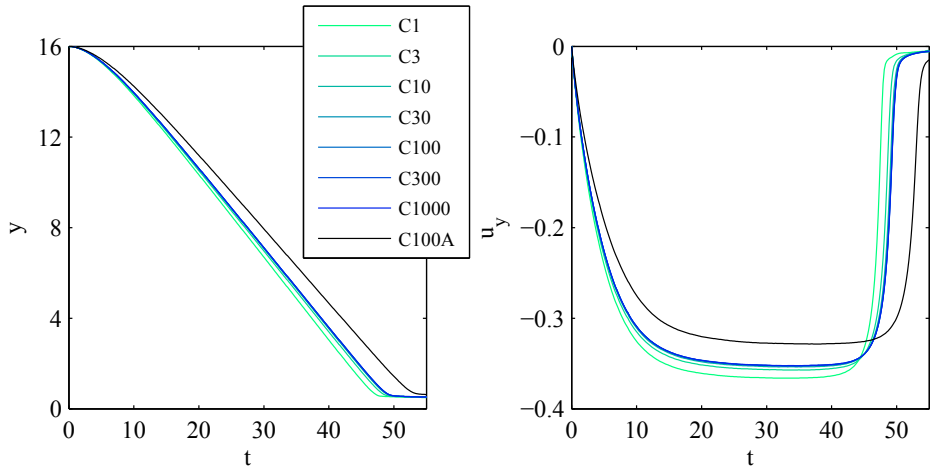

Figure 2: Vertical position (left) and vertical velocity (right) of the solid disk's center of mass versus time for all test cases.

Table 2: Time and vertical velocity of solid disk's center of mass at $y = 6$ for all test cases

Case	C1	C3	C10	C30	C100	C300	C1000	C100A
t	31.8981	32.7057	33.0270	33.1203	33.1550	33.1600	33.1680	35.9186
u_y	-0.3662	-0.3572	-0.3537	-0.3528	-0.3525	-0.3524	-0.3524	-0.3283

tours of the solid disk when case C100 is at $y = 6$, during its descent at terminal velocity. The differences between profiles become negligible for viscosity ratios above 100. Time until the disks reach $y = 6$ and their terminal velocity at the same height are provided for all test cases in table 2.

In conjunction with viscosity ratio, the interpolation scheme used to transition through phase boundaries affects the outcome of the simulation as well. To demonstrate this effect, WAM scheme is compared to WHM scheme. In WAM, the transition occurs at equal distances at both sides of the phase boundaries whereas in WHM the transition is skewed toward the higher–valued material property. As higher viscosity generates larger skin friction, it is desired to avoid transition in fluid domain as much as possible. In this sense the use of WAM, which generates a thicker region of higher viscosity inside the fluid domain than WHM, hinders the descent of the disk. Simulation results presented in figures 2, 3 and table 2 bear out the observation that the WAM case lags behind all WHM cases.

Based on the observations made above, a viscosity ratio of 100 with WHM interpolation scheme has been chosen and the results are provided in figure 4. The right portion of the figure provides velocity vectors and contours of velocity magnitude on the left column and streamlines and pressure contours on the right column at $y = 6$, when the disk

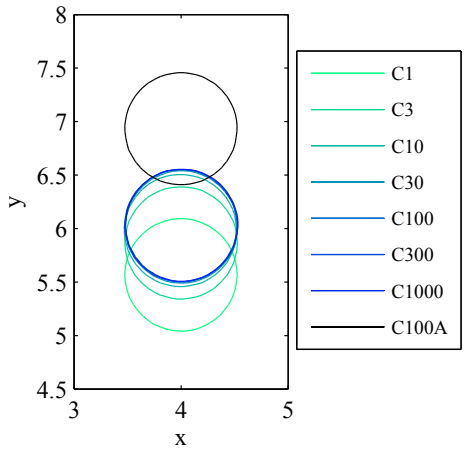

Figure 3: Disk position for all test cases when C100 is at $y = 6$.

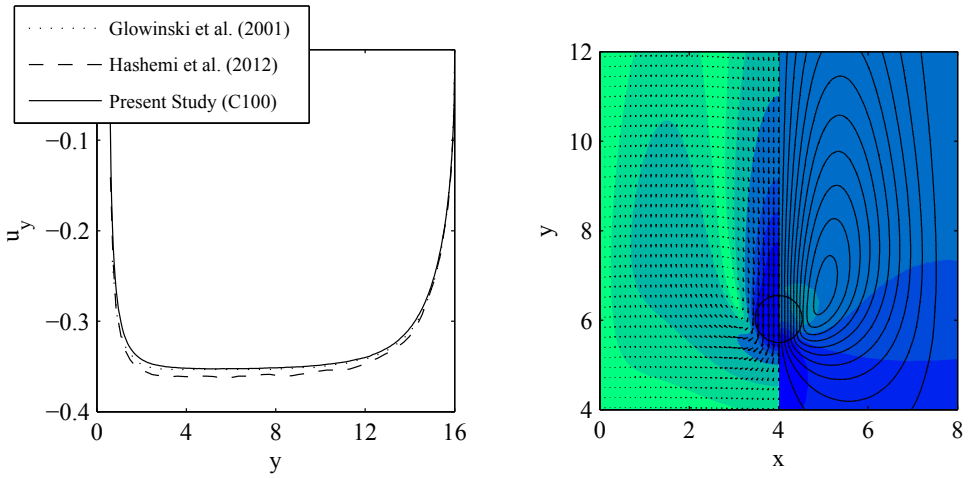

Figure 4: (Left) Comparison of vertical velocity of solid disk's center of mass with respect to its vertical position. (Right) Close up of the disk at $y = 6$, descending at its terminal velocity; Left Column: velocity vectors and contours of velocity magnitude; Right Column: streamlines and pressure contours.

is descending at its terminal velocity. Figure 4–left shows the comparison of vertical velocity versus vertical position of the disk's center of mass compared with the Weakly Compressible SPH (WCSPH) simulations of Hashemi *et al.* [13] and fictitious domain approach of Glowinski *et al.* [1]. Our scheme is able to capture the motion of the disk within the quiescent medium with quantitative accuracy.

5 CONCLUSION

In this paper, we have presented an ISPH–based method for simulating the motion of a passive solid in a body of fluid. The effects of viscosity ratio and interpolation scheme on the performance of the proposed scheme for simulation of a descending solid disk in quiescent medium are evaluated. The simulation data with properly matched parameters are found to be in agreement with previous results in the literature.

6 ACKNOWLEDGMENTS

The authors gratefully acknowledge financial support provided by the Scientific and Technological Research Council of Turkey (TUBITAK) for project number 112M721.

REFERENCES

[1] Glowinski, R., Pan, T., Hesla, T., Joseph, D. and Periaux, J. A fictitious domain approach to the direct numerical simulation of incompressible viscous flow past moving rigid bodies: Application to particulate flow. *J. Comput. Phys.* (2001) **169**:363–426.

[2] Balaras, E. Modeling complex boundaries using an external force field on fixed Cartesian grids in large-eddy simulations. *Comput. Fluids* (2004) **33**:375–404.

[3] Zhang, Y., Zou, Q., Greaves, D., Reeve, D., Hunt-Raby, A., Graham, D., James, P. and Lv, X. A level set immersed boundary method for water entry and exit. *Commun. Comput. Phys.* (2010) **8**:265–288.

[4] Oger, G., Doring, M., Alessandrini, B. and Ferrant, P. Two-dimensional SPH simulations of wedge water entries. *J. Comput. Phys.* (2006) **213**:803–822.

[5] Kajtar, J. and Monaghan, J. SPH simulations of swimming linked bodies. *J. Comput. Phys.* (2008) **227**:8568–8587.

[6] Shao, S. Incompressible SPH simulation of water entry of a free-falling object. *Int. J. Numer. Methods Fluids* (2009) **59**:91–115.

[7] Cummins, S. and Rudman, M. An SPH projection method. *J. Comput. Phys.* (1999) **152**:584–607.

[8] Koshizuka, S., Nobe, A. and Oka, Y. Numerical analysis of breaking waves using the moving particle semi-implicit method. *Int. J. Numer. Methods Fluids* (1998) **26**:751–769.

[9] Monaghan, J.J. and Lattanzio, J.C. A refined particle method for astrophysical problems. *Astron. Astrophys.* (1985) **149**:135–143.

[10] Monaghan, J.J. and Kocharyan, A. SPH simulation of multiphase flow. *Comput. Phys. Commun.* (1995) **87**:225–235.

[11] Zainali, A., Tofighi, N., Shadloo, M.S. and Yildiz, M. Numerical investigation of Newtonian and non-Newtonian multiphase flows using ISPH method. *Comput. Meth. Appl. Mech. Eng.* (2013) **254**:99–113.

[12] Yildiz, M., Rook, R.A. and Suleman, A. SPH with the multiple boundary tangent method. *Int. J. Numer. Methods Eng.* (2009) **77**:1416–1438.

[13] Hashemi, M., Fatehi, R. and Manzari, M. A modified SPH method for simulating motion of rigid bodies in Newtonian fluid flows. *Int. J. Non-Linear Mech.* (2012) **47**:626–638.